Polymeric Microcapsules as Robust Mimics of Emulsion Liquid Membranes for Selective Ion Separations

Jay R. Werber[1,2,*], Colin Peterson[1], Dean F. Stipanic[2], and Marc A. Hillmyer[1,*]

[1]*Department of Chemistry, University of Minnesota, Minneapolis, Minnesota, 55455, USA*

[2]*Department of Chemical Engineering & Applied Chemistry, University of Toronto, Toronto, M5S 3E5, Canada*

*Corresponding authors:

Marc Hillmyer, hillmyer@umn.edu, Phone: 612-625-7834

Jay Werber, jay.werber@utoronto.ca, Phone: 416-978-4906

Abstract

Selective ion separations are increasingly needed to combat water scarcity, recover resources from wastewater, and enable the efficient recycling of electronics waste. Emulsion liquid membranes (ELMs) have received interest due to rapid kinetics, high selectivities, and low solvent requirements, but are too unstable for industrial usage. We demonstrate that polymeric microcapsules can serve as robust, solvent-free mimics of ELMs. As a proof of concept, we incorporated the copper-selective ligand Lix 84-I in the walls of microcapsules formed from a commercial polystyrene-*b*-polybutadiene-*b*-polystyrene triblock polymer. The microcapsules were formed from a double-emulsion template, resulting in particles typically 20–120 μm in diameter that encapsulated even smaller droplets of a dilute (≤ 0.5 M) H_2SO_4 solution. Batch experiments demonstrated facilitated-transport behavior, with equilibrium reached in as little as 10 min for microcapsules with 1% ligand, and with ~15-fold selectivity for Cu^{2+} over Ni^{2+}.

Furthermore, the microcapsules could be packed readily in columns for flow-through operation, thus enabling near-complete Cu^{2+} removal in ~2 min under certain conditions, recovery of Cu^{2+} by flowing through fresh dilute H_2SO_4, and reuse for at least 10 cycles. The approach in this work can serve as a template for using selective ligands to enable robust and simple flow-through processes for a variety of selective ion separations.

Keywords

Selective ion separations, facilitated transport membranes, resource recovery, wastewater treatment, hydrometallurgy, microcapsules, extraction

Synopsis

Selective removal and recovery of metal ions is needed for efficient wastewater treatment. This study reports a robust and reusable microcapsule platform in which selective ligands carry ions to the capsule interior.

Table of Contents Graphic

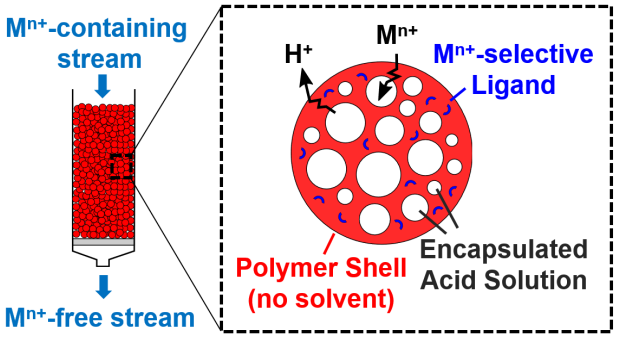

Introduction

Climate change and challenges at the water-energy-food nexus require innovations that help build sustainable, circular economies.[1] Water and natural resources like metals are increasingly important. Our use of metals has also grown increasingly complex. For example, a single mobile phone today likely contains >70 different elements, most of which are metals.[2] This complexity hinders responsible life-cycle management; many metals have near-zero rates of recycling, while many others are not produced domestically, putting supply chains at risk.[3] Additionally, aqueous solutions of metal ions are often toxic (e.g., those containing lead or mercury). Wastewater from the mining sector, for example, must be managed to limit environmental exposure to toxic ions, while treatment processes with limited ion/ion selectivity and high energy needs, such as reverse osmosis, are typically used for these applications.[4,5] Improved processes for selective ion separations are needed to address these challenges.[5,6]

The premier technology for separating dissolved ions of similar size and charge density is currently liquid/liquid extraction—also called solvent extraction (SX)—which is used in industrial hydrometallurgical operations.[7,8] In SX, a lipophilic ligand (also called an extractant) dissolved in an organic phase selectively complexes a target metal ion at or near the solvent/water interface, extracting the ion from the aqueous phase. The metal-ion-loaded organic phase is then contacted with a secondary aqueous strip solution to recover the ions and regenerate the free ligand. In many processes, aqueous solution pH is used to drive extraction and stripping, with metal ions being exchanged for protons in the stripping process. While SX enables highly selective separations, it has several important drawbacks, including a large solvent inventory, potential for environmental release of solvent, phase-separation issues (e.g., emulsion formation), and the required stoichiometric binding of ligands with ions.[9] The latter can be costly when using complex,

extraordinarily selective ligands such as the macrocyclic calixarenes used in SX to remove radioactive cesium from legacy nuclear-industry waste by the US Department of Energy.[10]

To address these issues, liquid-based facilitated transport membranes were explored extensively in the 1980's and 1990's, with research continuing to the present.[9,11–13] In these membranes, the ligand-containing organic phase is placed between the aqueous feed and strip solutions, coupling the two steps, with the ligands serving as carriers to shuttle ions between the two aqueous solutions. Critically, the membranes break the stoichiometric relationship between ligands and extracted ions in SX, as the driving force for transport of ions instead becomes related to differences in co-ion (especially H^+ for many cations) or counter-ion concentrations in the aqueous feed and strip solutions; the membrane ligand content instead mostly impacts the transport kinetics.[9,13] In other words, dramatically reduced ligand amounts are required for facilitated transport membranes compared to SX. At the same time, the selectivity of facilitated transport membranes approaches that of SX with the same ligand,[9] enabling ion/ion selectivities that cannot be achieved using conventional size-based and charge-based membranes.

Liquid-based facilitated transport membranes can be formed as either planar membranes (supported liquid membranes) or dispersed droplets. The dispersed form, called emulsion liquid membranes (ELMs), received substantial academic and industrial interest, largely owing to their rapid kinetics.[13–16] In this format, a water-in-oil-in-water (W/O/W) double emulsion is formed, with the oil phase forming a heterogeneous membrane separating the outer feed solution from the encapsulated strip solution (often a solution of sulfuric acid). The double emulsion would be formed and broken with every extraction/stripping cycle. While the high surface areas of ELMs enable rapid extraction kinetics, the complex processing and instability of the system have

hindered industrial adoption. Other capsule-based approaches that have been explored (e.g., liposomes) are also unstable.[17,18]

Polymeric systems offer the potential for enhanced robustness, while essentially eliminating solvent usage.[13,19,20] For example, there has been substantial interest in planar polymer inclusion membranes (initially called gelled supported liquid membranes[21]), which are typically mixtures of glassy polymers (e.g., cellulose triacetate or polyvinyl chloride), plasticizer, and extractant.[19,20] The plasticizers are needed, often at high levels (20–70%), to increase diffusivity.[19] Recently, the triblock polymer polystyrene-*b*-polybutadiene-*b*-polystyrene (SBS) was used as the base material for a polymer inclusion membrane, in the absence of plasticizer.[22] Although not discussed in that work, we expect that the low glass-transition temperature (T_g) of polybutadiene (≈ –90 °C for a mostly 1,4 microstructure sample[23]) would enable paths of increased diffusivity, with the polystyrene blocks providing physical crosslinks to enable robustness. While SBS is a promising material for polymer-based facilitated transport membranes, the planar format hindered kinetics, with several hours required for complete separations—even for membranes with high levels of ligand (e.g., 30 wt% Lix 84-I).[22]

In this work, we use double-emulsion templating to form SBS microcapsules that serve as robust, polymeric mimics of ELMs, which we also refer to as dispersible polymeric facilitated transport membranes. To demonstrate this approach, we incorporated Lix 84-I—a phenolic oxime that selectively extracts Cu^{2+}—into the microcapsule walls, while encapsulating sulfuric acid at concentrations up to 0.5 M. Crucially, the system is essentially solvent-free with the exception of a small amount of hydrocarbon diluent present in the Lix 84-I reagent. Batch experiments demonstrated rapid kinetics, with equilibrium reached in ~10 min for microcapsules with 1 wt% Lix 84-I in the walls. These experiments demonstrated selective uptake of Cu^{2+} over Ni^{2+} and

facilitated transport of Cu^{2+} to the microcapsule interior, with total uptake up to 77-fold greater than expected for direct ligand/ion extraction alone. The polymer microcapsule approach also enables regenerable column operation, with Cu^{2+} able to be selectively taken up and then fully recovered in at least 10 cycles. While this proof-of-concept study targeted Cu^{2+} uptake, the approach should be modifiable to target a variety of aqueous metal ions, simply by changing the incorporated ligand.

Materials & Methods

Materials. The polystyrene-*b*-polybutadiene-*b*-polystyrene polymer D1157 was kindly supplied by Kraton. Lix 84-I was kindly supplied by BASF. Polyvinyl alcohol (M ~ 13–23 kg/mol, 87–89% hydrolyzed) was purchased from Sigma-Aldrich. The monomer *n*-propyl styrene sulfonic ester (SSE) was synthesized according to literature procedures.[24,25] The chain transfer agent 2-(Dodecylthiocarbonothioylthio)-2-methylpropionic acid (DDMAT) was synthesized according to literature procedures.[26,27] All other chemicals were purchased from Sigma-Aldrich.

Synthesis of PI-PSSA. Polyisoprene-*b*-poly(*n*-propyl styrene sulfonic ester) (PI-PSSE) was synthesized through reversible addition/fragmentation chain-transfer (RAFT) polymerization as a precursor to the amphiphilic diblock polymer polyisoprene-*b*-poly(styrene sulfonic acid) (PI-PSSA), which was used to stabilize water-in-oil emulsions during microcapsule preparation. Polyisoprene (PI) was first synthesized following literature procedures.[26,28] In short, 0.625 mmol of DDMAT (1 molar equiv), distilled isoprene, and 0.125 mmol of *tert*-butyl peroxide (0.2 equiv) were charged into a 150-mL pressure vessel, sparged on ice with Ar for 25 min, and quickly capped. After sparging, 27.2 g (400 mmol, 640 equiv) isoprene remained. The pressure vessel was then placed in a pre-heated 125 °C oil bath for 22.5 h, with magnetic stirring. The reaction was then

cooled and precipitated 2x from dichloromethane (DCM) into methanol. A small amount of butylated hydroxytoluene (BHT) was added to prevent crosslinking, after which the polymer was dried overnight in a vacuum oven at 60 °C to yield 4.8 g of yellow, viscous liquid.

Using polyisoprene as a macro-chain transfer agent (macroCTA), PI-PSSE was synthesized based on literature procedures.[24] PI macroCTA (1 g, 0.089 mmol, 1 equiv) and SSE (2.67 mmol, 30 equiv) were dissolved in 4 mL tetrahydrofuran (THF) and passed through a basic alumina plug to remove stabilizers, with the solution collected in a 2-dram septum vial. Azobisisobutyronitrile (AIBN, 0.018 mmol, 0.2 equiv) was then added, and the reaction was sparged with Ar for 20 min. The vial was then placed in a 60 °C aluminum well, with magnetic stirring, for 7 days. The polymer was purified by precipitating twice from THF into methanol. A small amount of BHT was added, and the polymer was dried in a vacuum oven overnight to yield 929 mg of yellow solid.

PI-PSSE was converted to PI-PSSA by reaction with an amine,[24] for which we used butylamine. PI-PSSE (855 mg) was dissolved in 5-mL THF in a 2-dram septum vial. The solution as sparged with Ar for 5 min on ice, then butylamine (1.5 mL) was added by needle through the septum, and the solution was sparged for 1 additional min. The vial was then allowed to mix at room temperature for 24 h. Residual butylamine and solvent were evaporated off, resulting in 845 mg of an orange, waxy solid.

Preparation of Microcapsules. An example microcapsule preparation procedure is described here. Lix 84-I (5.4 mg), 18 mg of PI-PSSA, 4 mL of 10 wt% SBS in DCM (~520 mg of SBS), and 1 mL of 0.5 M H_2SO_4 in water were added to a 50-mL polypropylene centrifuge tube. The tube was vortexed for 2 min to form a coarse emulsion, after which the solution was placed on ice and then probe sonicated with 10 s on/10 s off for 10 min total time using a QSonica Q55, 50W sonicator with CL-188 horn and 1/8" probe tip diameter. After sonication, this water-in-oil (DCM) emulsion

was thick (viscous), white, and opaque. A 20-mL solution of 2% (w/v) PVA, 0.4 M NaCl was then poured into the centrifuge tube, which was then homogenized for 1 min at room temperature to form a water-in-oil-in-water double emulsion using a Fisher Sci Powergen 125 Homogenizer with 5-mm generator (probe) operating at 8000 rpm. The solution was then poured immediately into a 500-mL solution of 0.1% (w/v) PVA, 0.4 M NaCl pre-heated to 30 °C and mixed using a magnetic PTFE stir bar. DCM was allowed to evaporate for ~1 h, after which 1.4 g of white microcapsules were recovered by vacuum filtration through a qualitative (1 μm pore size) paper filter (Fisher P5). Microcapsules were used immediately or stored in 0.5 M H_2SO_4 for later use. The NaCl concentration was chosen to roughly balance the osmotic pressure with the internalized H_2SO_4 solution. For 0.1 M H_2SO_4 and 0.02 M H_2SO_4, NaCl concentrations of 80 mM and 16 mM were used, respectively.

Ion Uptake Experiments. In batch experiments, a given mass of microcapsules was mixed with 15-mL of ion-containing solution. For each timepoint, 0.3 mL of the suspension was removed using a micropipette and filtered immediately through a glass wool plug to remove microcapsules. The filtrate was analyzed colorimetrically for ion concentration. For column experiments, 400 mg of microcapsules were dispersed in 0.4 M NaCl and flow packed into a glass Pasteur pipet plugged with glass wool. After flow-packing, glass wool was added to the top of the column bed to minimize disruption of the column packing during liquid changes. The column was then connected to a syringe pump to enable consistent flow rates. Solutions in the syringe pump were changed manually, and the effluents from the columns were collected in vials or tubes for later analysis. Columns were stored in 0.5 M H_2SO_4 between runs, matching the inner solution for the relevant microcapsules.

Ion Quantitation. Copper and nickel were quantified colorimetrically using a UV/Vis spectrophotometer (Shimadzu), loosely following literature procedures.[29,30] For Cu^{2+} measurements, Cu^{2+} concentrations were quantified at 272 nm using polyethyleneimine (PEI) as a reagent. Immediately before absorbance measurements, 1 mL of phosphate buffer (0.1 M KH_2PO_4, 0.18 M Na_2HPO_4, pH 7.0), 50 μL of 10 wt% PEI, 200–950 μL of sample, and deionized water were added to make 2 mL total volume. For Ni^{2+} measurements, 100 μL of sample, 100 μL deionized water, 200 μL of 3% (w/v) dimethylglyoxime in 1 M NaOH, and 800 μL 2 M NaOH were mixed and allowed to complex for 3 h at room temperature. Sonication was not found to affect color intensity, in contrast to literature claims.[30] Immediately prior to absorbance measurements, 1 mL of this mixture was mixed with 1 mL of deionized water. Absorbance was quantified at 466 nm. Both of the above procedures produced linear relationships between absorbance and concentration in the range of interest. For some column runs, samples were analyzed using inductively coupled plasma-optical emission spectroscopy (ICP-OES), using an iCap 7600 Duo instrument.

Other Characterization. Nuclear magnetic resonance (NMR) spectroscopy was conducted on a Bruker Advance III HD 500 spectrometer. Chemical shifts are reported in δ units, expressed in ppm downfield of tetramethylsilane, using residual $CHCl_3$ peak as an internal standard ($CDCl_3$, ^1H: 7.26 ppm). Size exclusion chromatography (SEC) was conducted in THF at 25 °C, 1 mL/min on an Agilent Infinity 1260 HPLC system equipped with three Waters Styragel HR columns in series, a Wyatt DAWN HELEOS-II 18-angle laser light scattering detector, and a Wyatt Optilab T-rEX differential refractive index detector. The dn/dc was estimated using the total mass recovery method. Differential scanning calorimetry (DSC) was conducted on a TA Instruments Discovery DSC using aluminum T-zero pans with hermetic lids. Infrared spectroscopy was conducted on a

Bruker Alpha Platinum ATR spectrometer with a diamond ATR crystal. Optical microscopy was conducted using an Amscope B120C-E5 microscope with a digital camera.

Results & Discussion

Design Criteria for Microcapsules as Dispersed Facilitated Transport Membranes. Before designing our system, we needed to determine the required properties to enable robust, rapid, and high-capacity ion separations. Ultimately, the design criteria for this system include (i) high acid stability, (ii) resistance to rupture under osmotic pressure differences, and (iii) maximal uptake kinetics. We discuss each criterion below.

Acid stability is needed to enable high concentrations of protons in the encapsulated strip solution, particularly if the driving force for metal ion uptake is ion exchange (i.e., M^{x+}/H^+ exchange). Disregarding the small quantity of ligand in the walls, the molar uptake of the target metal ion, $n_{M^{x+}}$, has an upper limit:[9]

$$n_{M^{x+}} \leq \frac{1}{x} c_{H^+} V_i \quad (1)$$

where c_{H^+} is the initial internal strip solution concentration of H^+ and V_i is the total internal volume of encapsulated strip solution. High concentrations of H^+ are therefore desirable to maximize the total uptake capacity of the system.

The second criterion—resistance to osmotic rupture—stems from this need for high acid concentrations in the encapsulated strip solution. For example, a 0.5 M H_2SO_4 solution has an osmotic pressure of 25 bar, calculated using the Pitzer model.[31] If a microcapsule that encapsulates 0.5 M H_2SO_4 is placed in a solution with low osmolarity, inward flow of water would eventually create a pressure difference, Δp, that matches the osmotic pressure difference. The maximum pressure, Δp_{max}, of spherical shells is given by the Laplace pressure:

$$\Delta p_{\max} = \frac{2\tau_R}{r} \quad (2)$$

where τ_R is the rupture tension of the wall material and *r* is the shell radius. Small internal cavities and high-strength shell walls are therefore important.

The third criterion is to maximize kinetics, for which we first need to consider the expected transport paths. Two possibilities exist: (i) ion transport while complexed to freely diffusing ligands and (ii) ion hopping between fixed ligands.[11] For the fixed-ligand scenario, ligands are only able to move on the nm-scale; the ligand sites must overlap to enable ion-hopping between sites or ions must be able to passively diffuse through the material to some extent.[11,32] The most common fixed-ligand scenario involves covalently tethering the ligand to the membrane matrix.

In the case of low concentrations of untethered ligand and a hydrophobic low-T_g (rubbery) matrix, the likely scenario is for ligands and ligand/ion complexes to freely diffuse through the wall material. This transport behavior should mirror that of liquid (carrier-based) facilitated transport membranes, which have been modeled extensively.[9,11,13] In these membranes, interfacial complexation/de-complexation reactions of ligands with the ions lead to sorption and desorption into and out of the membrane phase. Transport is then diffusive, with ligand/ion complexes diffusing from the feed side to the strip side, and free ligands diffusing the other direction. For a ligand/metal complexation such as the Cu^{2+}/Lix 84-I system in this study, the complexation reaction is described by:[14]

$$Cu^{2+} + 2RH \leftrightarrow CuR_2 + 2H^+ \quad (3)$$

where RH is the free ligand and CuR_2 is the ligand/Cu^{2+} complex at a ratio of 2:1. The free ions are in the aqueous phase, while the free ligand and ligand/ion complexes are in the membrane phase. The resulting equilibrium constant, *K*, is:[14]

$$K = \frac{\{CuR_2\}\{H^+\}^2}{\{Cu^{2+}\}\{RH\}^2} \quad (4)$$

where K is a product of the activities. Assuming local equilibrium is reached at each interface,[33] eq 4 would apply for both the outer (feed) and inner (strip) sides of the shell. Rearranging eq 4 gives the relation

$$\frac{\{CuR_2\}}{\{RH\}^2} = K\frac{\{Cu^{2+}\}}{\{H^+\}^2} \quad (5)$$

wherein the ratio of complexed ligand activity to the square of the free ligand activity is given. For a microcapsule system at equilibrium, the activities of free ligand and ligand/ion complexes are uniform in the membrane, giving us the relation:[9]

$$\{Cu^{2+}\}_S = \left(\frac{\{H^+\}_S}{\{H^+\}_F}\right)^2 \{Cu^{2+}\}_F \quad (6)$$

The subscripts F and S refer to the feed and strip solutions, respectively. Following eq 6, if the equilibrium pH of the strip solution is 1 pH unit lower than the feed solution, then the Cu^{2+} activity in the strip solution is expected to be 100-fold greater than that in the feed. This result is similar to that for Donnan Dialysis,[33] except that in facilitated transport the ligands (carriers) enable sharply enhanced ion selectivity.

Following the solution-diffusion model,[34] if we assume that diffusion in the membrane is rate-limiting—a common assumption for liquid membranes[9,13,33]—and the activity coefficient for the ligands and ligand/ion complexes are constant in the membrane, then we can write the flux of Cu^{2+} across the wall, J, as:[35]

$$J = (D/\delta)([CuR_2]_F - [CuR_2]_S) \quad (7)$$

where $[CuR_2]_F$ and $[CuR_2]_S$ are the ligand/ion complex concentrations in the membrane at the feed and strip interface, respectively, D is the mutual diffusion constant for the ligand/ion complex in the membrane phase, and δ is the local thickness of the capsule wall.

Based on eqs 4–7, we can qualitatively analyze system properties that would maximize flux. High diffusivities for the ligand/ion complex are clearly desired, which is challenging due to the

relatively large size of most complexes (>>100 g/mol) and the need for high τ_R to maximize resistance to rupture. Small wall thicknesses are desired, which again is contrary to rupture resistance. The third component to increasing flux is to increase the gradient of ligand-ion complex within the capsule wall. Based on eq 5, increasing the total quantity of ligand (i.e., $2[CuR_2] + [RH]$) would increase the concentration of ligand/ion complex and the resulting gradient in eq 7. That said, given that one of the main advantages of the approach is to minimize the amount of required ligand, it may be more beneficial to keep the ligand quantity low, particularly for costly, highly selective ligands.[8,10]

Choice of Materials and Proposed Transport Path. Based on the above design criteria, we chose SBS as the base polymer to form the walls of the microcapsules. SBS is a commonly used thermoplastic elastomer that self-assembles into ordered nanoscale domains, with the polystyrene end-blocks forming glassy polymeric domains that physically crosslink the material.[36] SBS is also relatively acid-stable and highly hydrophobic, which should minimize permeation of free (uncomplexed) ions. The material we used (Kraton D1157) is 70 wt% polybutadiene (equivalent to 82% of monomer units and a volume fraction of 0.73), with the remainder polystyrene (Figure S1). The polybutadiene was predominantly (87%) 1,4 microstructure based on NMR analysis and we expect the glass transition temperature to be low (Figure S2).[23] The low T_g of polybutadiene should contribute to high diffusivities with a relatively weak dependence on molar mass of the permeant,[33,37] which is especially important given the large size of ligand/ion complexes.[7]

In principle, the microcapsule approach could target a wide variety of metal ion species, with the selectivity of the system determined by the ligand choice.[9,19] We chose the Cu^{2+}-selective ligand Lix 84-I for our proof of concept,[7,14,22] as previous work had demonstrated that SBS and Lix 84-I were miscible up to high levels (~30 wt% Lix 84-I)[22] and copper could be readily

quantified using colorimetric techniques (Figure S3).[29] The active (Cu^{2+}-binding) component of Lix 84-I is 2-hydroxy-5-nonylacetophenone oxime (HNAPO), with the remainder of the Lix 84-I mixture proprietary but largely comprising a hydrocarbon diluent.[7,38] Purification of HNAPO[38] from the Lix 84-I led to a 57% reduction in protons corresponding to the aliphatic region by NMR analysis, consistent with removal of a hydrocarbon diluent (Figure S4). Solvent extraction tests performed using Lix 84-I in $CHCl_3$ suggested that HNAPO comprises 45 wt% of the Lix 84-I mixture (Figure S5), assuming 1:2 coordination of Cu^{2+}:HNAPO.[14] We used the Lix 84-I mixture directly, as previous work with Lix 84-I and SBS suggested that the unpurified mixture had better performance compared to HNAPO.[22]

To determine the equilibrium morphology of the system, we performed small-angle x-ray scattering (SAXS) on solid SBS films with Lix 84-I content varying from 0–20 wt% (Figure 1A). The scattering pattern observed was characteristic of hexagonally packed cylinders for all samples, with minimal change in scattering behavior. Based on the principal scattering peak, the center-to-center spacings of adjacent cylinders remained relatively invariant, with ~39-nm spacing for pure SBS and ~38-nm for SBS with 20 wt% Lix 84-I. Small reductions in domain spacing are expected to occur for certain block polymers as solvent content increases.[39]

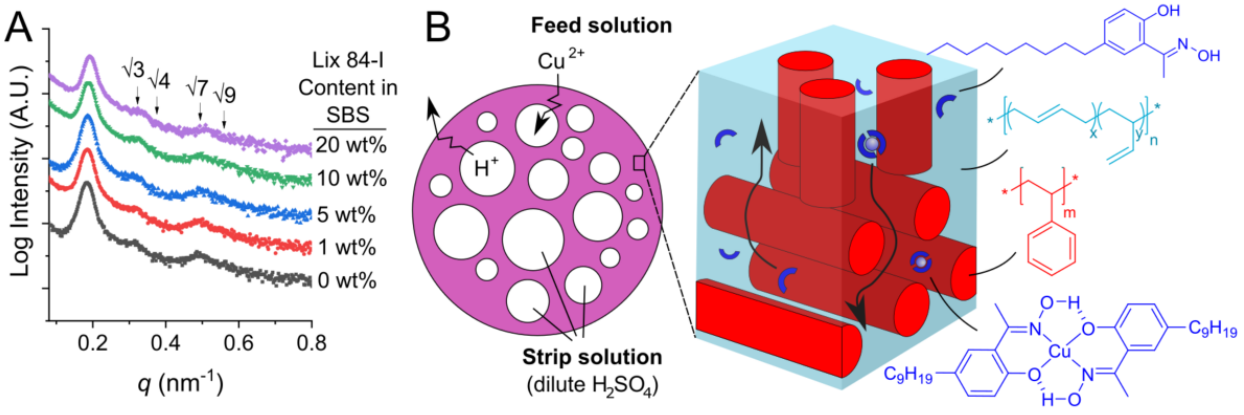

Figure 1. Polymer nanostructure and schematic of ion transport. (A) Small angle x-ray scattering of poly(styrene)-*b*-poly(butadiene)-*b*-poly(styrene) (SBS) block polymer mixed with the copper-

binding ligand Lix 84-I, showing a scattering pattern characteristic of cylindrical microphases. (B) Schematic of the expected ion transport behavior in metal-selective SBS microcapsules. During extraction, Cu^{2+} is transported to inner droplets, while H^+ is transported the reverse direction. Free ligands and ion/ligand complexes diffuse through the rubbery polybutadiene phase.

Based on this cylindrical morphology, Figure 1B depicts the expected transport behavior for the system. As described in the next section, the microcapsules formed contained multiple inner droplets of encapsulated strip solution. Cu^{2+} ions are transported through the membrane walls into these inner droplets, with H^+ transported the opposite direction. Within the walls itself, the polystyrene end-blocks form cylindrical domains that physically crosslink the system, enhancing mechanical robustness. Polystyrene is glassy ($T_g \approx 100$ °C) and highly impermeable to solutes with sizes similar to HNAPO;[35] any ligand that is dissolved in the polystyrene phase likely contributes minimally to Cu^{2+} flux. The polybutadiene phase, in contrast, would enable high diffusivity, and critically, should be continuous throughout the material (Figure 1B). Transport continuity is often a technical challenge for porous materials derived from block polymers, given that pores must typically be formed from the minority phase.[40] In this system, using polybutadiene as the majority phase enables continuity while also retaining 73% of the volume as the desired diffusion path. It is worth emphasizing that the self-assembly behavior of the triblock polymer SBS is essential to simultaneously enable physical robustness and fast transport—two properties that would be difficult to achieve in a homopolymer system without post-modification (i.e., crosslinking).

Preparation of Acid-Filled, Ligand-Containing Microcapsules. Polymer microcapsules encapsulating aqueous solutions can be formed in a variety of ways. A common approach in the literature is through microfluidics, which enables precise formation of microcapsules with nearly uniform capsule diameters and typically a single aqueous cavity.[41–43] The most industrially scalable approach is through bulk double-emulsion templating, in which a W/O/W double

emulsion is first formed through homogenization, after which evaporation of the solvent leaves behind the polymeric shell.[44,45] This approach typically results in microcapsules with varying diameters and multiple internal aqueous cavities. For simplicity and given our need to produce relatively large quantities of microcapsules for metal uptake experiments, we elected to use the bulk double-emulsion templating approach.

The procedure used to prepare the polymeric microcapsules is shown in Figure 2A. We first formed a water-in-oil (W/O) emulsion through probe sonication on ice of dilute H_2SO_4 solutions in a solution of DCM, SBS polymer, and Lix 84-I. The organic:aqueous volumetric ratio was fixed at 4:1. To stabilize the W/O emulsion, we synthesized amphiphilic polyisoprene-*b*-poly(4-styrene sulfonic acid) (PI-PSSA) diblock polymers using RAFT polymerization, building on strategies we have previously explored.[24,26] The reactions are described in Schemes S1 and S2, with polymer characterization shown in Figures S6-S11. The chemistries were chosen due to the expected compatibility of PI with the polybutadiene in the SBS shell, the relative acid stability of PI and PSSA, and the water solubility of PSSA. Additionally, we did not expect the protonated (uncharged) or deprotonated (negatively charged) PSSA to significantly hinder Cu^{2+} transport, while deprotonated PSSA could even contribute to total Cu^{2+} uptake. The number-average molar mass (M_n) for the PI and PSSA blocks were 11 kg/mol and 4.6 kg/mol, respectively (Table S1). The greater chain length for PI compared to PSSA was chosen to facilitate inward curvature of water droplets and thereby stabilize the W/O emulsion (Figure 1A), analogous to surfactants with a low hydrophilic-lipophilic balance (HLB).[46–48] The PI-PSSA was highly effective at stabilizing the W/O emulsion, with ~20 mg of polymer used for 1 mL of aqueous solution and 4 mL of organic solution. The emulsion did not separate after several days at room temperature. In contrast, >200 mg of small-molecule surfactant with low HLB (Span 85) was needed to stabilize the equivalent

system, with some emulsion breakage occurring within hours. Based on analysis of the W/O/W droplets (Figures 2B, S12), the water droplets in the PI-PSSA-stabilized W/O emulsion had diameters mostly < 6 μm (Figure S13).

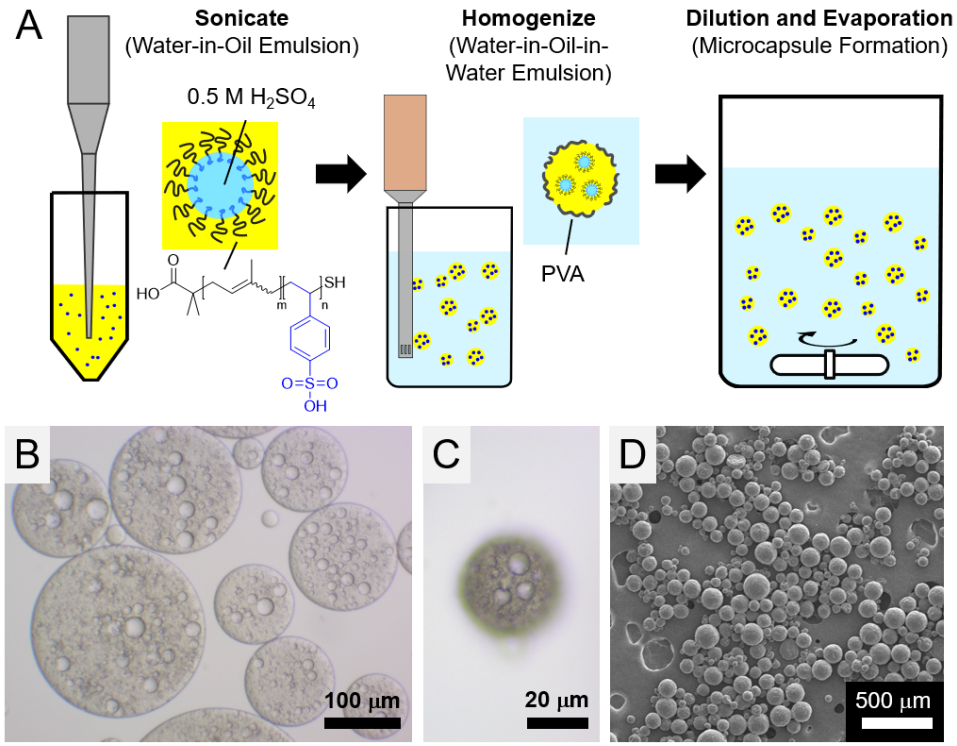

Figure 2. Preparation of ligand-containing polymeric microcapsules encapsulating dilute sulfuric acid. (A) Schematic showing formation of water-in-oil-in-water (W/O/W) emulsions, with subsequent removal of the DCM solvent to form microcapsules with solid walls. (B-C) Optical micrographs of the (B) W/O/W emulsion and (C) microcapsule, with 0.5 M H_2SO_4 as the internal solution and 1 wt% Lix 84-I, relative to the capsule wall. (D) Electron micrograph of dried microcapsules.

To form the W/O/W emulsion, a 20-mL solution of 2% (w/v) PVA with NaCl was added to the W/O emulsion, followed by homogenization at 8000 rpm. PVA is an acid-stable polymeric surfactant, while NaCl was added to balance osmotic pressure with the internal droplets. This procedure resulted in large W/O/W double-emulsion droplets, which we visualized using optical

microscopy (Figures 2B, S12). To form solid microcapsules, the solvent must be removed. W/O/W emulsions are intrinsically unstable;[48] for our system, despite the highly stable initial W/O emulsion, the loss of inner droplets to the continuous (outer) aqueous phase could be observed in real-time via optical microscopy. More quantitatively, we found through preliminary experiments with $CuSO_4$-filled microcapsules that rapid removal of DCM by diluting the W/O/W emulsion into a 500-mL solution sharply reduced ion leakage to 20%, compared to 70% for a W/O/W emulsion allowed to evaporate DCM overnight without the dilution step (Figure S14). The dilution step rapidly extracted DCM from the microcapsules,[44] given the solubility of DCM with water (16 g/L at 30 °C). After filtering, this procedure resulted in solid microcapsules with encapsulated aqueous droplets of dilute H_2SO_4, as visualized by optical microscopy (Figures 2C, S15, S16) and SEM (Figure 2D). Microcapsules were heterogeneous in size, with most having diameters of 20–120 μm (Figure S17), and remained well-dispersed if mixed in solution. If stored dry in a capped vial, microcapsules would agglomerate; they were therefore used immediately or stored in a dilute H_2SO_4 solution with H_2SO_4 concentration matching the internal solution. Measurement of the filtrate pH during microcapsule recovery enabled an estimation of the encapsulation efficiency of H_2SO_4, which was typically ~30%. To determine encapsulation efficiency, the filtrate pH was compared with a titration curve for the outer solution with increasing additions of H_2SO_4. Given that the outer volume and total H_2SO_4 added to the system were known (e.g., 520 mL outer volume and 1 mL of 0.5 M H_2SO_4), comparison of the filtrate pH with the titration curve enabled estimation of H^+-leakage and, in turn, H^+-encapsulation. Encapsulation of H_2SO_4 was lower than for $CuSO_4$ (~80% encapsulation, Figure S14), possibly due to differing emulsion stabilities as PSSA is largely neutrally charged at pH < 1.

Batch Experiments Show Internalization of Metal Ions Driven by Outward Proton Gradient. To demonstrate facilitated transport with the microcapsules, we recovered microcapsules by filtration and mixed 50–200 mg of microcapsules with 15 mL of 1 mM $CuSO_4$, 20 mM NaMES, pH 5.6. The results of these model experiments are shown in Figures 3A and 4. Uptake was very rapid, with equilibrium uptake achieved in as little as 10 min. Additionally, uptake remained relatively stable over 120 min of mixing. In other words, the Cu^{2+} that was taken up by the microcapsules was stably removed, with only relatively minor levels of Cu^{2+} leakage from the particles. The minimal leakage is notable, given the up to ~24-bar osmotic pressure difference between the encapsulated strip solution (up to 0.5 M H_2SO_4) and the buffered $CuSO_4$ solution. The general profile of ion uptake is similar to those for the most successfully demonstrated ELM systems, with similar kinetics for our samples with 1 wt% Lix in the microcapsule walls (Figure 4) as a Lix-based ELM with 10 wt% Lix reagent that was also targeting copper uptake.[14]

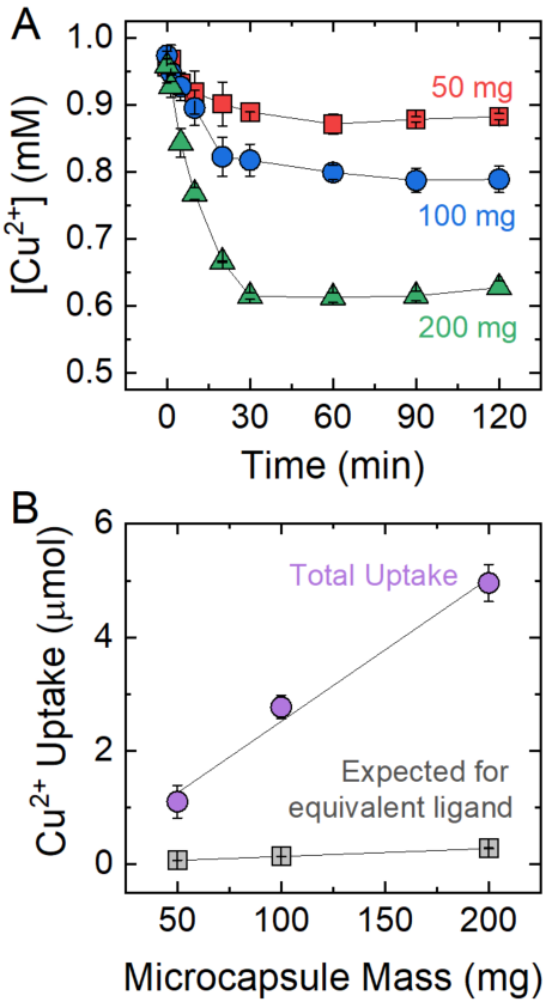

Figure 3. Batch uptake of Cu^{2+} into microcapsules. (A) Transient curves of Cu^{2+} concentration in the feed (outer) solution. (B) Cu^{2+} uptake into microcapsules, with total uptake based on $[Cu^{2+}]$ at 0 min and 120 min. The squares refer to the expected Cu^{2+} uptake for extraction using the mass of Lix 84-I present in the microcapsules, based on SX experiments (Figure S5). For each batch experiment, microcapsules with 0.5 wt% Lix 84-I in the walls were mixed with 15 mL of 1 mM $CuSO_4$, 20 mM NaMES, pH 5.6. All experiments were done in duplicate, with error bars depicting the range of data. Each replicate used a freshly prepared batch of microcapsules.

Figure 3B shows a comparison of the total Cu^{2+} uptake with the expected uptake for extraction with an equivalent mass of Lix 84-I that was present in the walls of the microcapsules, based on solvent extraction experiments done under the same conditions (Figure S5). The uptake increases proportionally with the mass of microcapsules added and was consistently 16–20-fold greater than

424 the expected uptake based on extraction alone. These results strongly support facilitated transport
425 to the inner droplets.

426 In further experiments, we varied the contents of the microcapsules, particularly the
427 concentration of Lix 84-I in the capsule walls and the acid concentration in the inner droplets
428 (Figure 4). The effect of ligand concentration on ion uptake is shown in Figure 4A. Capsules with
429 no ligand showed minimal uptake, with a small (~0.02 mM) drop from the initial concentration
430 occurring immediately and no further uptake over 120 min. This small Cu^{2+} uptake is likely due
431 to electrostatic binding with sulfonate groups in PI-PSSA that are exposed to the outer solution
432 (buffered at pH 5.6), possibly through defects formed during microcapsule preparation. These
433 "defects" likely formed through the merging of inner droplets with the outer solution, as observed
434 by optical microscopy. As the Lix 84-I concentration increased to 1%, the rate of Cu^{2+} uptake
435 increased linearly (Figure S18), in accordance with eq 5. The microcapsules reached their steady-
436 state values at approximately 10, 30, and 120 min for 1, 0.5, and 0.1 wt% Lix 84-I, respectively.
437 The total amount of Cu^{2+} taken up was similar between the three samples, with the microcapsules
438 with 0.1 wt% Lix 84-I taking up 4.0 μmol Cu^{2+} compared with 5.2 μmol Cu^{2+} for microcapsules
439 with 1 wt% Lix 84-I. The total Cu^{2+} uptake for the samples with 0.1 wt% Lix 84-I was 77-fold
440 greater than expected for ligand extraction alone.

441 The effect of internal acid concentration is shown in Figure 4B. In contrast to ligand
442 concentration, the internal acid concentration impacted the total uptake, while the rate of Cu^{2+}
443 uptake—particularly the initial slope—was unaffected. The total uptake increased non-linearly
444 with acid concentration, with the 5-fold concentration increase from 100 to 500 mM H_2SO_4 only
445 increasing uptake 1.8-fold (Figure S19). The non-linear response is likely partially due to the PSSA
446 lining internal droplets contributing to Cu^{2+} uptake. The estimated maximum Cu^{2+} binding (i.e., 1

447 Cu^{2+} per 2 sulfonates) to internalized PSSA would contribute to ~0.14 mM Cu^{2+} uptake in these
448 experiments, which is comparable to the drop for the sample prepared with 20 mM H_2SO_4.
449 The batch experiments show Cu^{2+} uptake in line with the facilitated transport mechanism:
450 greater ligand resulted in faster kinetics with small changes in total uptake while greater internal
451 acid concentrations during preparation led to greater uptake with no change in kinetics. To further
452 analyze kinetics, we modeled the results using eqs 4 and 7 and some simplifying assumptions, as
453 described fully in the Supporting Information, with the facilitated-transport model depicted as solid
454 lines in Figure 4. The model fit the data well, using a common SBS wall thickness and a common
455 ligand diffusivity for all curves and adjusting the starting internal H_2SO_4 concentration for each
456 curve to account for variability in encapsulation efficiency. For the samples formed with 0.5 M
457 H_2SO_4, the model suggests initial H_2SO_4 concentrations were ~40 mM H_2SO_4, corresponding to
458 an encapsulation efficiency of ~8% (Table S4), which is less than the ~30% efficiency estimated
459 using pH measurements during microcapsule preparation. While the cause of this discrepancy is
460 unknown, one possibility is acid being released during the copper uptake experiments (e.g., due to
461 osmotic bursting of some of the cavities).
462

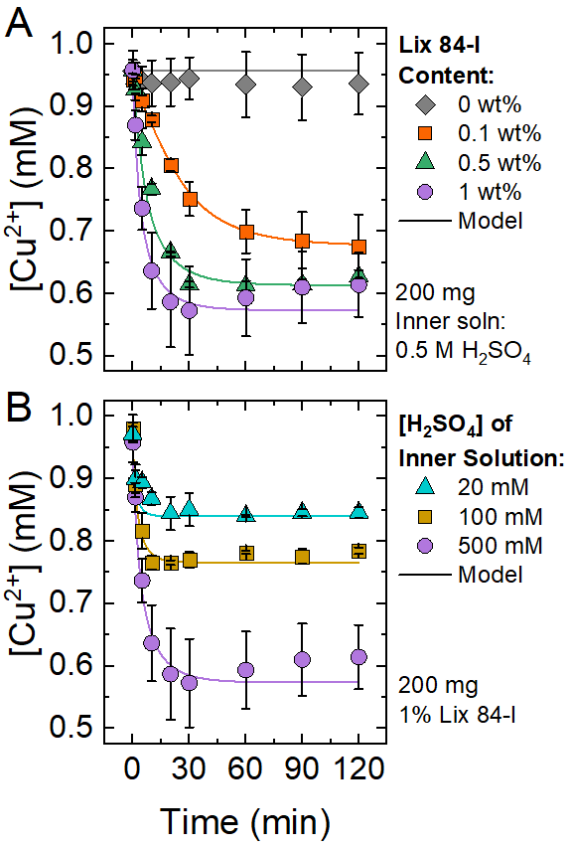

463

464 **Figure 4.** Batch uptake of Cu^{2+} into microcapsules for varying (A) ligand content as wt% of
465 microcapsule walls and (B) internal acid content. For each experiment, microcapsules were mixed
466 with 15 mL of 1 mM $CuSO_4$, 20 mM NaMES, pH 5.6. All experiments were done in duplicate,
467 with error bars depicting the range of data, except for the 1 wt% Lix 84-I, 500 mM H_2SO_4 sample,
468 which was run in triplicate, with error bars depicting standard deviation. Each replicate used a
469 freshly prepared batch of microcapsules. The solid lines depict model results, as described in the
470 Supporting Information. Model parameters are listed in Tables S3 and S4.
471

472 **Microcapsules Show Selective Metal Ion Uptake.** The above experiments targeted Cu^{2+} uptake
473 in the presence of just a buffer solution. To demonstrate ion/ion selectivity, we performed similar
474 experiments with mixed solutions of 1 mM $CuSO_4$ and 1 mM $NiSO_4$, buffered at pH 5.6 as in
475 Figures 3 and 4 and at pH 4.0 (Figure 5). Lix 84-I binds Cu^{2+} more strongly than Ni^{2+}, with Cu^{2+}
476 extracted preferentially, especially at lower pH (Figure S20). Cu^{2+} and Ni^{2+} were again quantified
477 colorimetrically, with relatively small interferences for mixed solutions in the assays (Figures S21-

S23). The presence of Ni^{2+} did not affect Cu^{2+} quantitation (Figure S21), while minor adjustments were made for Ni^{2+} quantitation based on the independently measured concentration of Cu^{2+} (Figure S23).

As shown in Figure 5, Cu^{2+} was selectively taken up by the microcapsules, with the Cu^{2+}/Ni^{2+} selectivities being 15 and 5.8 for pH 5.6 and 4.0, respectively, when comparing concentrations at 0 min and 120 min for the mixed feeds. The Cu^{2+} uptake curves for mixed feeds mirrored the uptake curves for solutions with just Cu^{2+} and buffer, except that the total Cu^{2+} uptake was slightly lower for mixed feeds, possibly due to Ni^{2+} uptake leading to H^{+} loss to the outer solution. The total Cu^{2+} uptake was also similar between the two pH levels.

Interestingly, the mixed and individual Ni^{2+} uptake curves were similar at pH 4.0, with a 0.05–0.07 mM decrease in Ni^{2+} concentration immediately upon microcapsule addition, followed by minimal further uptake. Considering that Ni^{2+} extraction by Lix 84-I is minimal at pH 4.0 (Figure S20), the rapid uptake and leveling off suggests that Ni^{2+} is binding non-specifically to the microcapsules, likely through interactions with PSSA that is exposed to the outer solution. This suggests that employing an uncharged surfactant to stabilize the inner droplets would increase the selectivities even further. The Ni^{2+} uptake behavior of the mixed feed at pH 5.6 was also indicative of interaction with PSSA, while the Ni^{2+} uptake for 1 mM $NiSO_4$ without Cu^{2+} showed a consistent and slow rate of uptake with final levels similar to the Cu^{2+} uptake experiments. This behavior can be rationalized by the partial (~80%) equilibrium extraction of Ni^{2+} by Lix 84-I at this pH level (Figure S20), in contrast to the essentially complete extraction of Cu^{2+}. The partial extraction would result in lower concentrations of ligand/ion complexes in the membrane phase, thereby decreasing flux (eq 7).

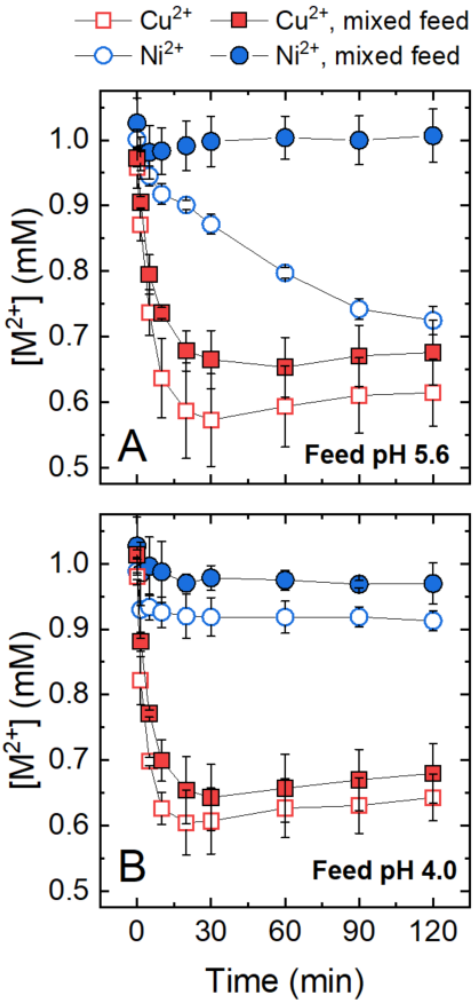

Figure 5. Selective Cu^{2+} uptake from mixed feed solution. Microcapsules (200 mg) were mixed with 15 mL of 1 mM $CuSO_4$ (open squares), 1 mM $NiSO_4$ (open circles), or a mixed solution of 1 mM $CuSO_4$ and 1 mM $NiSO_4$ (closed symbols). Solutions were buffered at (A) pH 5.6 using 20 mM NaMES and (B) pH 4.0 using 20 mM NaAcetate. Cu^{2+} was selectively removed at both pH levels (solid symbols). All experiments were done in duplicate, with error bars depicting the range of data. Each replicate used a freshly prepared batch of microcapsules, which were prepared with 1 wt% Lix 84-I and internal solutions of 0.5 M H_2SO_4.

Column Packing Enables Near-Complete Metal Removal. While the batch experiments enabled insight into uptake kinetics and selectivity, the batch format was difficult to use in a process, especially at lab-scale. Filtration of the solution to separate the microcapsules from the outer solution inevitably led to microcapsule loss, which prohibited regeneration and recovery of

514 the captured metal ions. One can imagine large-scale use of the microcapsule format in suspension,
515 with submerged porous ultrafiltration or microfiltration membranes retaining the microcapsules in
516 the vessel, similar to how microbes are retained in a membrane bioreactor.[49]

517 The other scaled-up format for which microcapsules could be readily employed is a packed
518 bed (i.e., a column), which could be readily cycled to enable metal ion uptake and regeneration,
519 similar to conventional ion exchange and emerging nanomaterial-based adsorbents.[50,51] The
520 packed-bed format is also easily reproduced at lab-scale. We prepared packed beds by flow
521 packing 400 mg of freshly prepared microcapsules—with 1 wt% Lix 84-I and 0.5 M H_2SO_4
522 internal solutions—into glass pipets that were plugged with glass wool. We then flowed 1 mM
523 $CuSO_4$, 20 mM NaMES, pH 5.6 solutions through the columns at a controlled flow rate (0.1
524 mL/min) using a syringe pump. Using dye as an indicator, we estimated the void volume of the
525 column to be 0.1–0.2 mL, suggesting a residence time of < 2 min for a flow rate of 0.1 mL/min.
526 After a certain feed volume was loaded, the columns were washed using 20 mM NaMES, pH 5.6,
527 and then the loaded Cu^{2+} ions were recovered by soaking the columns overnight in fresh 0.5 M
528 H_2SO_4.

529 As shown in Figures 6 and S24, the column format enabled essentially complete removal of
530 Cu^{2+} from the buffered solution before break-through, despite the short residence time of < 2 min.
531 We normalized the feed volume to the expected extraction based on the amount of ligand in the
532 microcapsules, which we did to emphasize the enhanced capacity conferred by the microcapsule
533 approach. For 1 mM $CuSO_4$ feeds, breakthrough occurred at a normalized load of 7–8 relative to
534 ligand (Figure 6A), which approached the 8.8-fold increase in uptake obtained for the same
535 microcapsules in batch experiments (Figure 3B). Below breakthrough, Cu^{2+} concentrations were
536 below the limit of detection of the colorimetric method (~0.006 mM). As shown in Figure 6B,

when the columns were soaked in fresh 0.5 M H_2SO_4, essentially all loaded Cu^{2+} could be recovered. Runs were also conducted with 0.1 mM $CuSO_4$ feeds, showing slightly diminished uptake capacity, but otherwise similar behavior. For the 0.1 mM $CuSO_4$ experiments, a small elution volume (2 mL) was used, enabling a ~30-fold concentration factor for Cu^{2+} (Figure 6C).

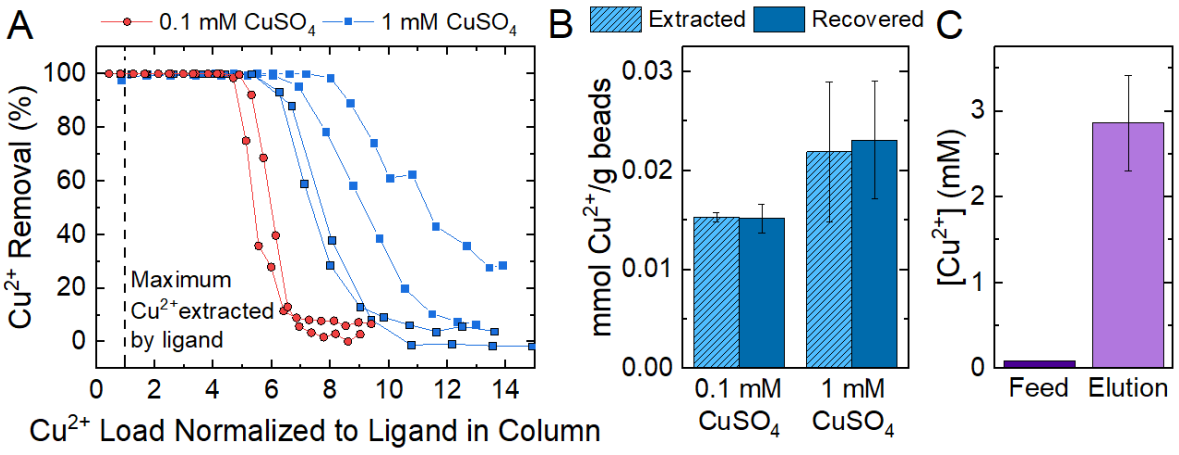

Figure 6. Uptake and recovery of Cu^{2+} using columns packed with microcapsules. (A) Cu^{2+} removal as a function of feed volume, which was normalized to the ligand mass present within the column. Unnormalized curves are presented in Figure S24. Each trace represents a unique column. Column residence time was ~2 min. Feed solution was 20 mM NaMES, pH 5.6 with 0.1 mM or 1 mM $CuSO_4$. (B) Total Cu^{2+} extracted from the feed and recovered in fresh 0.5 M H_2SO_4 strip solution. (C) Cu^{2+} concentrations in the feed and elution solutions for the 0.1 mM $CuSO_4$ runs. Columns contained 400 mg of microcapsules with 1 wt% Lix 84-I and 0.5 M H_2SO_4 internal solution. Error bars reflect the range of values for duplicate samples or standard deviation of four replicates. Flow rate was 0.1 mL/min. Copper was recovered by flowing 2–10 mL of fresh 0.5 M H_2SO_4 through the column, with an overnight pause halfway through the elution.

In principle, the recovery of loaded metal ions with fresh strip solution should simultaneously regenerate the encapsulated strip solution (i.e., replace Cu^{2+} in the inner droplets with H^+), enabling reuse of the columns. To test reusability, we ran 10 cycles with a column, wherein the column was loaded in each cycle with a normalized load of ~5-fold greater than would be extracted using the column ligand content. We chose this level to be sufficiently below breakthrough to enable near-

559 complete Cu^{2+} removal, based on Figure 6A. Load flow rate was set to 0.1 mL/min, while the
560 strip/regeneration time varied from 100 min (10 mL at 0.1 mL/min) to overnight. Cycles with 100-
561 min strip times were run the same day, while 1-day strip times were due to the column being stored
562 in strip solution overnight before the next cycle.

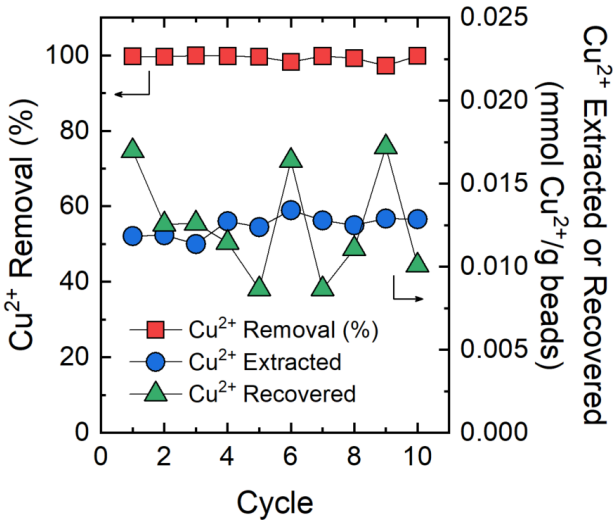

563

564 **Figure 7**. Reuse and regeneration of a column packed with microcapsules. The column contained
565 400 mg of microcapsules with 1 wt% Lix 84-I and 0.5 M H_2SO_4 internal solution. The column
566 was fed with 1 mM $CuSO_4$, 20 mM NaMES, pH 5.6 at 0.1 mL/min (~2 min residence time),
567 washed with ~3-mL 20 mM NaMES, pH 5.6, and then stripped/regenerated using fresh 0.5 M
568 H_2SO_4. Regeneration time varied between 100 min (cycles 5, 7, 8, and 10) and 1 day (cycles 1–4,
569 6, and 9). Prior to cycle 1, the column was used for breakthrough analysis as a column in Figure
570 6.
571

572 As shown in Figure 7, the column was able to be effectively reused, maintaining near-complete
573 Cu^{2+} removal over ten cycles. The amount of Cu^{2+} extracted remained relatively constant, with
574 slight fluctuations owing to variability in the mass of Cu^{2+} that was loaded onto the column. The
575 recovered Cu^{2+} was slightly more variable, with the recovered amount exceeding the amount
576 extracted in certain cycles and the opposite result in other cycles. This variability in Cu^{2+} recovery
577 was due to the varying strip/regeneration time, which again varied from 100 min to 1 day. The
578 data suggests that 100 min was not enough time for complete Cu^{2+} recovery. For example, cycles

5, 7, and 8 were stripped for 100 min, after which cycles 6, 8, and 9 were started immediately. The incomplete Cu^{2+} stripping led to decreased effective capacity for Cu^{2+} uptake in the next cycle, resulting in partial breakthrough and removals of 98.3%, 99.3%, and 97.3% for cycles 6, 8, and 9, respectively. While these removal rates remained high, they were the only cycles above the detection limit for the colorimetric assay (Table S2). Higher Cu^{2+} recovered masses were achieved in these cycles, due to the inadequate stripping in the previous cycle. While we did not fully explore the kinetics of stripping, it is notable how much slower stripping is than for Cu^{2+} uptake at pH 5.6, which is complete within 2 min. The slower kinetics of stripping/regeneration are likely due to the low pH on both sides of the capsule walls, leading to a relatively low proportion of ligand being complexed to Cu^{2+}.

To assess the absolute levels of Cu^{2+}, the raffinates (i.e., the flow-through during the feed step) from the reuse study were analyzed by inductively coupled plasma-optical emission spectroscopy (ICP-OES) for Cu^{2+} and Na^{+} concentrations, where the sodium came from the NaMES buffer. The low Cu^{2+} levels in these samples led to imprecise measurements in the colorimetric assay, which is not as sensitive. The ICP-OES measurements found that cycles 1-4 and cycle 10 were below the effective limit of detection for Cu^{2+}, which was 0.0006 mM (Table S2). This equates to >99.95% removal. The ICP-OES measurements also found that Na^{+} concentrations were unchanged going from the feed to the raffinate, suggesting that Cu^{2+}/Na^{+} selectivities are extremely high.

Outlook for Microcapsules as Dispersible Facilitated Transport Membranes. In this work, we demonstrated that polymeric microcapsules with selective ligands dissolved in the capsule walls could enable highly selective and rapid ion separations. For expediency, we chose Cu^{2+} as a target metal ion to be transported using a commercial ligand from hydrometallurgy (mining), but we envision the main application of this approach to be resource recovery of high-value metals from

dilute wastewaters, particularly using complex, costly, and highly selective ligands. The ability to break the stoichiometric relationship between ligand and ion is particularly valuable in that respect. The 1% ligand capsules that we used most frequently increased uptake 9-fold over pure ligand/ion extraction, while the 0.1% ligand capsules enabled a 77-fold increase in uptake, albeit with slower kinetics. The other main benefit of this approach is the ability to conduct solvent-free processing in column formats or dispersed in vessels. The increased safety and flexibility offered by solvent-free processing is advantageous.

Going forward, it will be valuable to explore even greater internal acid concentrations and optimize encapsulation efficiencies to further increase the metal uptake capacity. The uptake capacity of ~0.02 mmol Cu^{2+}/g wet beads for our microcapsules is lower than common ion exchange resins that bind ~3 meq/g wet beads.[52] Given that our encapsulation efficiencies were ~8% based on modeling and ~30% based on pH measurements, sharply improved uptake capacities are likely possible with improved microcapsule fabrication and higher internal sulfuric acid concentrations (e.g., >1 M). In terms of fundamental behavior, ion-uptake kinetics matched a facilitated-transport model for mobile carriers. While sorption and diffusion of similar solutes in similar polymers have been measured,[37] *in situ* measurements of ligand diffusion in SBS are needed to confirm the diffusive transport behavior.

For the system we explored with Lix 84-I, Cu^{2+} uptake in columns was rapid (complete in < 2 min), but the regeneration/stripping step was slow due to lower ion/ligand complex concentrations at low pH. Increased uptake capacity would decrease the frequency needed for regeneration, and applications with dilute feeds (e.g., resource recovery from wastewater) that do not need frequent regeneration should be prioritized. Systems should also be explored for which regeneration can be done more rapidly. Lastly, exploration of alternative emulsion-stabilizing polymeric surfactants

will be useful, particularly using neutrally charged (yet acid-stable) hydrophilic blocks, to eliminate non-specific binding of ions to exposed internal cavities.

Associated Content

Supporting Information

The Supporting Information is available free of charge on the ACS Publications website at DOI: 10.1021/XXXX

1st File: NMR and SEC of SBS triblock polymer (Figure S1); DSC thermograms of SBS with and without Lix 84-I incorporation (Figure S2); Calibration for colorimetric measurement of Cu^{2+} (Figure S3); NMR of as-received and purified Lix 84-I (Figure S4); Solvent extraction of Cu^{2+} using Lix 84-I to determine uptake capacity (Figure S5); Polymerization of PI-PSSE (Scheme S1); Deprotection of PI-PSSE to form PI-PSSA (Scheme S2); Molar masses and relative compositions of synthesized polymers (Table S1); NMR of PI macroCTA (Figure S6); NMR of PI-PSSE1 (Figure S7); NMR of PI-PSSE2 (Figure S8); SEC of PI macroCTA and PI-PSSE (Figure S9); FTIR spectra of PI macroCTA, PI-PSSE1, and PI-PSSA1 (Figure S10); FTIR spectra of PI macroCTA, PI-PSSE2, and PI-PSSA2 (Figure S11); Optical micrographs of double emulsions (Figure S12); Size distribution of inner droplets (Figure S13); Leakage of inner ions during optimization of microcapsule preparation (Figure S14); Optical micrographs of SBS microcapsules (Figures S15-S16); Size distribution of microcapsules (Figure S17); Copper uptake rates in batch experiments with SBS microcapsules with varying ligand wt% (Figure S18); Total copper uptake in batch experiments with SBS microcapsules with varying H_2SO_4 concentration in inner droplets (Figure S19); Batch extraction of Cu^{2+} and Ni^{2+} using SBS films with Lix 84-I and varying pH (Figure S20); Colorimetric measurement of Cu^{2+} in presence of Ni^{2+} (Figure S21);

Calibration for colorimetric measurement of Ni^{2+} (Figure S22); Colorimetric measurement of Ni^{2+} in presence of Cu^{2+} (Figure S23); Column Cu^{2+} removal based on volumetric throughput (Figure S24); Ion concentrations measured using ICP-OES and colorimetric assay for column reuse experiments (Table S2); Transport model simplification to 1-dimensional transport (Figure S25); Estimation of equilibrium coefficient for Cu^{2+} uptake (Figure S26); Comparison of experimental data and models (Figure S27); Full model output (Figure S28); Parameters used during modeling (Table S3); Effective encapsulation ratios (Table S4).

2nd file: Python code used for numerical modeling.

Author Information

Corresponding Authors

*E-mail hillmyer@umn.edu (M. A. H.); jay.werber@utoronto.ca (J. R. W.)

ORCID

Marc A. Hillmyer: 0000-0001-8255-3853

Jay R. Werber: 0000-0002-6551-5983

Colin Peterson: 0000-0003-4250-4330

Dean F. Stipanic: 0000-0002-7012-7897

Notes

The authors declare no competing financial interest.

Acknowledgements

Funding for this work was provided by the Department of Energy (BES Award DE-SC0020210). Parts of this work were carried out in the Characterization Facility, UMN, which receives partial support from NSF through the MRSEC program. We also thank Hyung Kae Lee for assistance with sample management.

References

(1) Shannon, M. a; Bohn, P. W.; Elimelech, M.; Georgiadis, J. G.; Mariñas, B. J.; Mayes, A. M. Science and Technology for Water Purification in the Coming Decades. *Nature* **2008**, *452* (7185), 301–310. https://doi.org/10.1038/nature06599.

(2) Rohrig, B. Smartphones: Smart Chemistry. *American Chemical Society*. 2015.

(3) Reck, B. K.; Graedel, T. E. Challenges in Metal Recycling. *Science* **2012**, *337* (6095), 690–695. https://doi.org/10.1126/science.1217501.

(4) Northey, S. A.; Mudd, G. M.; Saarivuori, E.; Wessman-Jääskeläinen, H.; Haque, N. Water Footprinting and Mining: Where Are the Limitations and Opportunities? *J. Clean. Prod.* **2016**, *135*, 1098–1116. https://doi.org/10.1016/j.jclepro.2016.07.024.

(5) Werber, J. R.; Osuji, C. O.; Elimelech, M. Materials for Next-Generation Desalination and Water Purification Membranes. *Nat. Rev. Mater.* **2016**, 16018. https://doi.org/10.1038/natrevmats.2016.18.

(6) *Basic Research Needs for Environmental Management*; Office of Science, Department of Energy, 2016; p 208.

(7) Wilson, A. M.; Bailey, P. J.; Tasker, P. A.; Turkington, J. R.; Grant, R. A.; Love, J. B. Solvent Extraction: The Coordination Chemistry behind Extractive Metallurgy. *Chem. Soc. Rev.* **2014**, *43* (1), 123–134. https://doi.org/10.1039/c3cs60275c.

(8) Moyer, B. A.; Bonnesen, P. V.; Custelcean, R.; Delmau, L. H.; Hay, B. P. Strategies for Using Host—Guest Chemistry in the Extractive Separations of Ionic Guests. *Kem. Ind.* **2005**, *54* (2), 65-87.

(9) Danesi, P. R. Separation of Metal Species by Supported Liquid Membranes. *Sep. Sci. Technol.* **1984**, *19* (11–12), 857–894. https://doi.org/10.1080/01496398408068598.

(10) Moyer, B. A.; Birdwell, J. F.; Delmau, L. H.; Duncan, N. C.; Ensor, D. D.; Hill, T. G.; Lee, D. L.; Roach, B. D.; Frederick, V.; Stoner, E. L.; Williams, N. J. *Next Generation Solvent Development for Caustic-Side Solvent Extraction of Cesium*; Dept. of Energy, 2014.

(11) Cussler, E. L.; Aris, R.; Bhown, A. On the Limits of Facilitated Diffusion. *J. Membr. Sci.* **1989**, *43* (2–3), 149–164. https://doi.org/10.1016/S0376-7388(00)85094-2.

(12) Reusch, C. F.; Cussler, E. L. Selective Membrane Transport. *AIChE J.* **1973**, *19* (4), 736–741. https://doi.org/10.1002/aic.690190409.

(13) Cussler, E. L. Facilitated Transport. In *Membrane Separation Systems: Recent Developments and Future Directions*; 1991.

(14) Raghuraman, B.; Tirmizi, N.; Wiencek, J. Emulsion Liquid Membranes for Wastewater Treatment: Equilibrium Models for Some Typical Metal-Extractant Systems. *Environ. Sci. Technol.* **1994**, *28* (6), 1090–1098. https://doi.org/10.1021/es00055a018.
(15) Raghuraman, B.; Tirmizi, N.; Wiencek, J. Emulsion Liquid Membranes for Wastewater Treatment Equilibrium Models for Lead- and Cadmium-Di-2-Ethylhexyl Phosphoric Acid Systems. *Environ. Sci. Technol.* **1995**, *29*, 979–984. https://doi.org/10.1021/es00055a018.
(16) Hu, S. Y. B.; Wiencek, J. M. Emulsion-Liquid-Membrane Extraction of Copper Using a Hollow-Fiber Contactor. *AIChE J.* **1998**, *44* (3), 570–581. https://doi.org/10.1002/aic.690440308.
(17) Shamsai, B. M.; Monbouquette, H. G. A23187-Mediated Cd 2+ Uptake by Highly Stable, Polymerized Metal-Sorbing Vesicles. *J. Membr. Sci.* **1997**, *130*, 173–181.
(18) Walsh, A. J.; Monbouquette, H. G. Extraction of Cd2+ and Pb2+ from Dilute Aqueous Solution Using Metal-Sorbing Vesicles in a Hollow-Fiber Cartridge. *J. Membr. Sci.* **1993**, *84* (1–2), 107–121. https://doi.org/10.1016/0376-7388(94)87027-6.
(19) Nghiem, L. D.; Mornane, P.; Potter, I. D.; Perera, J. M.; Cattrall, R. W.; Kolev, S. D. Extraction and Transport of Metal Ions and Small Organic Compounds Using Polymer Inclusion Membranes (PIMs). *J. Membr. Sci.* **2006**, *281* (1–2), 7–41. https://doi.org/10.1016/j.memsci.2006.03.035.
(20) Almeida, M. I. G. S.; Cattrall, R. W.; Kolev, S. D. Recent Trends in Extraction and Transport of Metal Ions Using Polymer Inclusion Membranes (PIMs). *J. Membr. Sci.* **2012**, *415–416*, 9–23. https://doi.org/10.1016/j.memsci.2012.06.006.
(21) Bromberg, L.; Levin, G.; Kedem, O. Transport of Metals through Gelled Supported Liquid Membranes Containing Carrier. *J. Membr. Sci.* **1992**, *71* (1–2), 41–50. https://doi.org/10.1016/0376-7388(92)85004-3.
(22) Xiong, X.; Almeida, M. I. G. S.; Simeonova, S.; Spassov, T. G.; Cattrall, R. W.; Kolev, S. D. The Potential of Polystyrene-Block-Polybutadiene-Block-Polystyrene Triblock Co-Polymer as a Base-Polymer of Polymer Inclusion Membranes (PIMs). *Sep. Purif. Technol.* **2019**, *229* (June), 115800. https://doi.org/10.1016/j.seppur.2019.115800.
(23) Richter, D.; Frick, B.; Farago, B. Neutron-Spin-Echo Investigation on the Dynamics of Polybutadiene near the Glass Transition. *Phys. Rev. Lett.* **1988**, *61* (21), 2465–2468. https://doi.org/10.1103/PhysRevLett.61.2465.
(24) Goldfeld, D. J.; Silver, E. S.; Radlauer, M. R.; Hillmyer, M. A. Synthesis and Self-Assembly of Block Polyelectrolyte Membranes through a Mild, 2-in-1 Postpolymerization Treatment. *ACS Appl. Polym. Mater.* **2020**, *2* (2), 817–825. https://doi.org/10.1021/acsapm.9b01100.
(25) Kolomanska, J.; Johnston, P.; Gregori, A.; Fraga Domínguez, I.; Egelhaaf, H. J.; Perrier, S.; Rivaton, A.; Dagron-Lartigau, C.; Topham, P. D. Design, Synthesis and Thermal Behaviour of a Series of Well-Defined Clickable and Triggerable Sulfonate Polymers. *RSC Adv.* **2015**, *5* (82), 66554–66562. https://doi.org/10.1039/c5ra13867a.
(26) Werber, J. R.; Peterson, C.; Zee, N. J. V.; Hillmyer, M. A. Functionalized Polymersomes from a Polyisoprene-Activated Polyacrylamide Precursor. *Langmuir* **2021**, *37*, 490–498.
(27) Lai, J. T.; Filla, D.; Shea, R. Functional Polymers from Novel Carboxyl-Terminated Trithiocarbonates as Highly Efficient RAFT Agents. *Macromolecules* **2002**, *43* (2), 122–123. https://doi.org/10.1021/ma020362m.

(28) Germack, D. S.; Wooley, K. L. Isoprene Polymerization via Reversible Addition Fragmentation Chain Transfer Polymerization. *J. Polym. Sci. Part Polym. Chem.* **2007**, *45*, 4100–4108. https://doi.org/10.1002/pola.22226.
(29) Wen, T.; Qu, F.; Li, N. B.; Luo, H. Q. A Facile, Sensitive, and Rapid Spectrophotometric Method for Copper(II) Ion Detection in Aqueous Media Using Polyethyleneimine. *Arab. J. Chem.* **2017**, *10*, S1680–S1685. https://doi.org/10.1016/j.arabjc.2013.06.013.
(30) Santos de Sousa, C.; Korn, M. Effects of Ultrasonic Irradiation on the Spectrophotometric Determination of Nickel with Dimethylglyoxime. *Anal. Chim. Acta* **2001**, *444* (2), 309–315.
(31) Pitzer, K. S.; Kim, J. J. Thermodynamics of Electrolytes. IV. Activity and Osmotic Coefficients for Mixed Electrolytes. *J. Am. Chem. Soc.* **1974**, *96* (18), 5701–5707. https://doi.org/10.1021/j100638a009.
(32) Moon, J. D.; Sujanani, R.; Geng, Z.; Freeman, B. D.; Segalman, R. A.; Hawker, C. J. Versatile Synthetic Platform for Polymer Membrane Libraries Using Functional Networks. *Macromolecules* **2021**, 54 (2), 866-873. https://doi.org/10.1021/acs.macromol.0c02414.
(33) Baker, R. W. *Membrane Technology and Applications*, 3rd ed.; Wiley, 2012.
(34) Rijnaarts, T.; Shenkute, N. T.; Wood, J. A.; de Vos, W. M.; Nijmeijer, K. Divalent Cation Removal by Donnan Dialysis for Improved Reverse Electrodialysis. *ACS Sustain. Chem. Eng.* **2018**, *6* (5), 7035–7041. https://doi.org/10.1021/acssuschemeng.8b00879.
(35) Wijmans, J. G.; Baker, R. W. The Solution-Diffusion Model: A Review. *J. Membr. Sci.* **1995**, *107* (1–2), 1–21. https://doi.org/10.1016/0376-7388(95)00102-I.
(36) Liffland, S.; Hillmyer, M. A. Enhanced Mechanical Properties of Aliphatic Polyester Thermoplastic Elastomers through Star Block Architectures. *Macromolecules* **2021**, *54* (20), 9327–9340. https://doi.org/10.1021/acs.macromol.1c01357.
(37) Siddaramaiah; Roopa, S.; Premakumar, U. Sorption and Diffusion of Aromatic Penetrants into Natural Rubber Blends. *Polymer* **1998**, *39* (17), 3925–3931. https://doi.org/10.1016/S0032-3861(97)10351-2.
(38) Warren, D. B.; Dyson, G.; Grieser, F.; Perera, J. M.; Stevens, G. W.; Rizzacasa, M. A. Characterisation of Nickel(II) Extraction by 2-Hydroxy-5-Nonylacetophenone Oxime (LIX 84) in a Micellar Phase. *Colloids Surf. Physicochem. Eng. Asp.* **2003**, *227* (1–3), 49–61. https://doi.org/10.1016/S0927-7757(03)00386-8.
(39) Naughton, J. R.; Matsen, M. W. Limitations of the Dilution Approximation for Concentrated Block Copolymer/Solvent Mixtures. *Macromolecules* **2002**, *35* (14), 5688–5696. https://doi.org/10.1021/ma0122066.
(40) Hampu, N.; Werber, J. R.; Chan, W. Y.; Feinberg, E. C.; Hillmyer, M. A. Next-Generation Ultrafiltration Membranes Enabled by Block Polymers. *ACS Nano* **2020**, *14* (12), 16446–16471. https://doi.org/10.1021/acsnano.0c07883.
(41) Datta, S. S.; Abbaspourrad, A.; Amstad, E.; Fan, J.; Kim, S. H.; Romanowsky, M.; Shum, H. C.; Sun, B.; Utada, A. S.; Windbergs, M.; Zhou, S.; Weitz, D. A. 25th Anniversary Article: Double Emulsion Templated Solid Microcapsules: Mechanics and Controlled Release. *Adv. Mater.* **2014**, *26* (14), 2205–2218. https://doi.org/10.1002/adma.201305119.
(42) Utada, A. S.; Lorenceau, E.; Link, D. R.; Kaplan, P. D.; Stone, H. A.; Weitz, D. A. Monodisperse Double Emulsions Generated from a Microcapillary Device. *Science* **2005**, *308* (5721), 537–541. https://doi.org/10.1126/science.1109164.

(43) Abbaspourrad, A.; Carroll, N. J.; Kim, S. H.; Weitz, D. A. Polymer Microcapsules with Programmable Active Release. *J. Am. Chem. Soc.* **2013**, *135* (20), 7744–7750. https://doi.org/10.1021/ja401960f.
(44) Yourdkhani, M.; Leme-Kraus, A. A.; Aydin, B.; Bedran-Russo, A. K.; White, S. R. Encapsulation of Grape Seed Extract in Polylactide Microcapsules for Sustained Bioactivity and Time-Dependent Release in Dental Material Applications. *Dent. Mater.* **2017**, *33* (6), 630–636. https://doi.org/10.1016/j.dental.2017.03.009.
(45) Shim, J. W.; Kim, S. H.; Jeon, S. J.; Yang, S. M.; Yi, G. R. Microcapsules with Tailored Nanostructures by Microphase Separation of Block Copolymers. *Chem. Mater.* **2010**, *22* (19), 5593–5600. https://doi.org/10.1021/cm101696t.
(46) Israelachvili, J. N. *Intermolecular and Surface Forces*; Academic Press: Boston, 2011.
(47) Walstra, P. Principles of Emulsion Formation. *Chem. Eng. Sci.* **1993**, *48* (2), 333–349. https://doi.org/10.1126/science.111.2874.82.
(48) Garti, N. Double Emulsions - Scope, Limitations and New Achievements. *Colloids Surf. Physicochem. Eng. Asp.* **1997**, *123–124*, 233–246. https://doi.org/10.1016/S0927-7757(96)03809-5.
(49) Yang, W.; Cicek, N.; Ilg, J. State-of-the-Art of Membrane Bioreactors: Worldwide Research and Commercial Applications in North America. *J. Membr. Sci.* **2006**, *270* (1–2), 201–211. https://doi.org/10.1016/j.memsci.2005.07.010.
(50) Luo, J.; Yu, D.; Hristovski, K. D.; Fu, K.; Shen, Y.; Westerhoff, P.; Crittenden, J. C. Critical Review of Advances in Engineering Nanomaterial Adsorbents for Metal Removal and Recovery from Water: Mechanism Identification and Engineering Design. *Environ. Sci. Technol.* **2021**, *55* (8), 4287–4304. https://doi.org/10.1021/acs.est.0c07936.
(51) Luo, J.; Crittenden, J. C. Nanomaterial Adsorbent Design: From Bench Scale Tests to Engineering Design. *Environ. Sci. Technol.* **2019**, *53* (18), 10537–10538. https://doi.org/10.1021/acs.est.9b04371.
(52) Chen, D.; Werber, J. R.; Zhao, X.; Elimelech, M. A Facile Method to Quantify the Carboxyl Group Areal Density in the Active Layer of Polyamide Thin-Film Composite Membranes. *J. Membr. Sci.* **2017**, *534*, 100–108. https://doi.org/10.1016/J.MEMSCI.2017.04.001.